Journal of Cleaner Production 509 (2025) 145601

Contents lists available at ScienceDirect

Journal of Cleaner Production

journal homepage: www.elsevier.com/locate/jclepro

Energy-driven decision support tool for friction stir additive manufacturing operations

Gianluca Buffa *, Simone Amantia, Davide Campanella, Giuseppe Ingarao, Livan Fratini

Department of Engineering, University of Palermo, Viale delle Scienze 90128, Palermo, Italy

ARTICLE INFO

Handling Editor: Jin-Kuk Kim

Keywords:
Friction stir welding
Additive manufacturing
Energy efficiency
Aluminum
Environmental impact

ABSTRACT

Friction Stir Additive Manufacturing (FSAM) allows the production of components by stacking and joining sheets via friction stir welding. FSAM's energy efficiency depends on the number of passes needed to achieve a specified build width. This study introduces a single-pass, pinless FSAM method for producing AA5754-H22 components. Mechanical tests showed performance comparable to traditional FSAM, with bonding efficiency between 91 % and 94 % of the base material. Energy evaluations for two industrial scenarios revealed that a pinless approach should be preferred over FSAM when a single-thickness approach is used with sheets of thicknesses lower than 4 mm. When a sheet thickness of 5 mm is considered, lower electrical energy consumption is obtained for build heights of 11 mm and higher. In a multi-thickness approach, the proposed approach is energetically effective with build height lower than 16 mm. Life Cycle Assessment (LCA) examined the environmental impact, including material considerations. The single-thickness pinless method (4 mm, 5 mm, and 1 mm cases) was analyzed using Cumulative Energy Demand (CED). For heights up to 18 mm, the pinless approach minimized or matched CED. However, for heights that are multiples of 5 mm, traditional FSAM showed advantages. At 17 mm, energy savings of 16 % and 9 % were achieved for 4 mm and 5 mm cases, respectively. In terms of Global Warming Potential, the pinless approach matched the single-thickness 4 mm case with an impact of 7.704 $kgCO_2$,eq. Overall, the pinless method is preferable for most target heights.

1. Introduction

Additive Manufacturing (AM) is a revolutionary technology which has been dramatically changing traditional manufacturing routes. This innovative approach has opened up new possibilities across various industries, ranging from aerospace and healthcare to automotive and consumer goods (Kruth et al., 1998). As compared to traditional manufacturing methods, AM not only reduces material waste but also facilitates the rapid prototyping of designs and customization of products with a huge impact on the manufacturing landscape and its potential to shape the future of production (Levy et al., 2003).

Fusion-based additive manufacturing processes, like selective laser melting (SLM) (Yi et al., 2020) or Electron Beam Melting (EBM) (Le et al., 2017), are being currently widely investigated and used in industry because of the tremendous possibilities that exist in terms of part design and geometrical complexity (Jones et al., 2021). However, these methods have certain limitations: (i) build size and speed, especially for powder-based processes (to a lesser extent for WAAM or DED processes) (Wang et al., 2022); (ii) thermal stress and distortion, due to the material melting and solidification, which can result in parts warping and poor dimensional accuracy; (iii) need for support structures requiring labor-intensive removal afterward and potentially causing surface imperfections; (iv) presence of melting related defects as porosities and cracks; (v) equipment costs and maintenance (Schmidt et al., 2017; Wits and Amsterdam, 2023).

Solid-state, friction-based additive processes have recently been developed to overcome some of the above-cited limitations. As solid-state processes, the lower temperatures significantly reduce residual stress and distortions. Besides, the compression-dominated process mechanics minimize the porosities issue making post-processing, as HIP treatments, unnecessary. Finally, simpler machines can be used, and large parts can be built with easiness. Currently, three main categories can be identified among solid-state friction-based additive processes: (i) processes based on friction surfacing, known as Additive Friction Stir Deposition (AFSD) (Stubblefield et al., 2022); (ii) processes based on friction stir extrusion, known as Friction Deposition (FD) or MELD after the company that patented the process (Gotawala and Yu, 2023); (iii) processes based on Friction Stir Welding (FSW), known as Friction Stir

* Corresponding author.
E-mail address: gianluca.buffa@unipa.it (G. Buffa).

https://doi.org/10.1016/j.jclepro.2025.145601
Received 4 September 2024; Received in revised form 29 January 2025; Accepted 25 April 2025
Available online 27 April 2025

Additive Manufacturing (FSAM) (Shao et al., 2023). In AFSD a consumable tool is rotated and pressed with an assigned force on a backplate. Then the tool is moved along a preset path. Depending on the combination of tool force, rotation, and feed rate, a layer of material from the tool will be deposited on the backplate (Hu et al., 2024). These processes have also been proven effective for cladding and repairing (Liu et al., 2016), although a quite large part of the tool is unusable after the process and must be recycled as scrap. In MELD a hollow non-consumable tool is used. Within the tool, a bar is fed and finally deposited between the tool's shoulder and the backplate. Although this process is extremely effective, allowing the production of high-quality parts (Rivera et al., 2018), it requires a dedicated machine partially canceling the advantages in terms of equipment costs and maintenance the solid-state processes usually have with respect to fusion-based processes. In FSAM sheets or plates are friction stir welded in a lap configuration creating a stack of the desired height (Rathee et al., 2021).

Recently, a few researchers have focused on the characterization of the FSAM process (Liu et al., 2024). The effectiveness of bonding at the interface between the layers of aluminum alloy AA 2195-T8 was investigated in (Zhao et al., 2019). Different tool pin shapes were tested, finding that the presence of the pin itself is critical to the integrity of the produced parts: both cylindrical and conical pin are not suitable for AFSD because of the presence of hooking defects which result in poor mechanical properties of the build, made of four layers with a thickness of 2 mm each. FSAM experiments on 4 mm thick AA5059 plates added with SiC reinforcement powder were carried out, showing the potential of the process also in producing MMCs (Srivastava and Rathee, 2021). FSAM principle was used to friction stir spot weld a stack of four 0.3 mm thin sheets using a specially designed convex tool in a unique process step (Labus Zlatanovic et al., 2020). Although promising, the approach was demonstrated only for spot welds.

From the literature analysis, it arises that, although post-processing machining is required, FSAM can allow to produce builds with fast material deposition rates due to the large "layer thickness" reachable, corresponding to the added sheet/plate thickness. Besides, no dedicated or complex machines are required. However, the presence of the pin can represent a problem, not only for the flow defects it induces but also because the width of the solid bonding between two layers is limited by the pin diameter itself, which usually has a tip diameter comparable to the considered sheet thickness (Zhao et al., 2019). In this way, when large structures must be produced, multiple passes are needed, losing part of the advantages the process has, also in terms of production time and energy footprint. In this paper, an approach based on FSAM using a pinless tool on 1 mm thick aluminum sheets is proposed to overcome the above-mentioned limitations. The mechanical properties of the builds are first examined. Then a comparison of the energy efficiency to conventional FSAM strategies is carried out to assess the validity of the presented approach. Finally, an LCA analysis was developed to better investigate the environmental impact of the traditional FSAM process and the pinless FSAM. This analysis was conducted following the structure outlined in ISO 14040.

2. Materials and methods

AA5754-H22 sheets, 1 mm in thickness were reduced to specimens with dimensions 175 mm × 75 mm and welded on a 6 mm thick backplate made of AA5083-H111 with the same planar dimensions. As mentioned, in order to get a large welding width, a pinless tool, made in H13 steel, was used. Fig. 1 shows the difference between the traditional FSAM process (Fig. 1a) and the pinless FSAM process (Fig. 1b).

Based on a preliminary experimental campaign, the thickness of the sheets to be used as "layers" was selected equal to 1 mm as the best compromise between the possibility to effectively use a pinless tool, resulting in larger widths of the weld seam with respect to pin tools, and the need to adopt a layer thickness as high as possible, thus maximizing the overall material deposition rate.

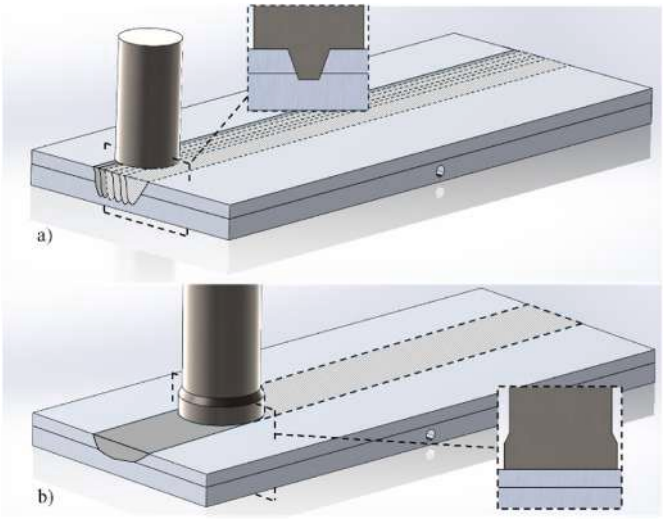

Fig. 1. (a) Sketch of the traditional FSAM process and (b) pinless FSAM process.

The process was carried out on an ESAB Legio machine for Friction Stir Welding, allowing force control of the tool. After the weldment of each layer, a milling operation is carried out, in the same machine and without unclamping the build, to eliminate the small flash at the sides of the weld seam and guarantee good contact conditions for the next layer. It is worth noting that the machine used for the FSAM process can be the same as the one considered for the milling process. In this way, the processed component remains in its assigned position once the milling process is completed, in order to have an automated production line. All the welds were carried out using a pinless tool with a 25 mm shoulder, constant force on the tool equal to 6 kN, tilt angle equal to 2°, and feed rate equal to 80 mm/min. Ten different layers were welded for each process condition, reaching a total nominal height of the build of 16 mm. As tool rotation is regarded, five different levels were considered, i.e. 500, 700, 900, 1100, and 1300 rpm. Based on the results of the preliminary campaign, different process parameters were used for the first layer, i.e. the one welded directly on the backplate, with respect to the ones used for all the remaining layers. In particular, regardless of the considered case study, the first layer was welded with a tool rotation equal to 2200 rpm to take into account the different welding conditions occurring. Each test was repeated three times.

During the process, temperature was acquired by embedding a K-type thermocouple in the backplate through a hole drilled on the lateral surface. Fig. 2a shows a sketch of the process with the thermocouple position, while in Fig. 2b the obtained build is shown. Fig. 2c shows the schematic representation of samples cut out of each produced build.

The energy consumption was measured by a Fluke 435 power quality analyzer able to measure voltage, current, and power over process time. Additional power and energy measurements were carried out using sheets of different thicknesses, keeping constant technological parameters, i.e. 2 mm, 3 mm, 4 mm, and 5 mm to assess energetic efficiency. For these sheets, a tool pin was needed in order to get proper bonding conditions. The dimensions of the utilized tools, all featuring a 30° conical pin, were selected based on the design rule derived from recent literature on FSAM (Table 1) (Lu and Reynolds, 2021; Jiang et al., 2023).

From each build a specimen was cut for a three-point bending test by milling the lateral parts of the sheets and reducing the actual built part to a 15 mm × 15 mm x 10 mm (L x W x H) protrusion over the backplate. Cross sections of the builds were observed by OM and SEM. The etching rate was determined by weight loss measurement after typical industrial processes, i.e. 10 min alkaline etching in the etching solution at 55 °C and 2 min desmutting in HNO_3 solution at room temperature. A miniaturized dog bone-shaped specimen, oriented perpendicularly to the

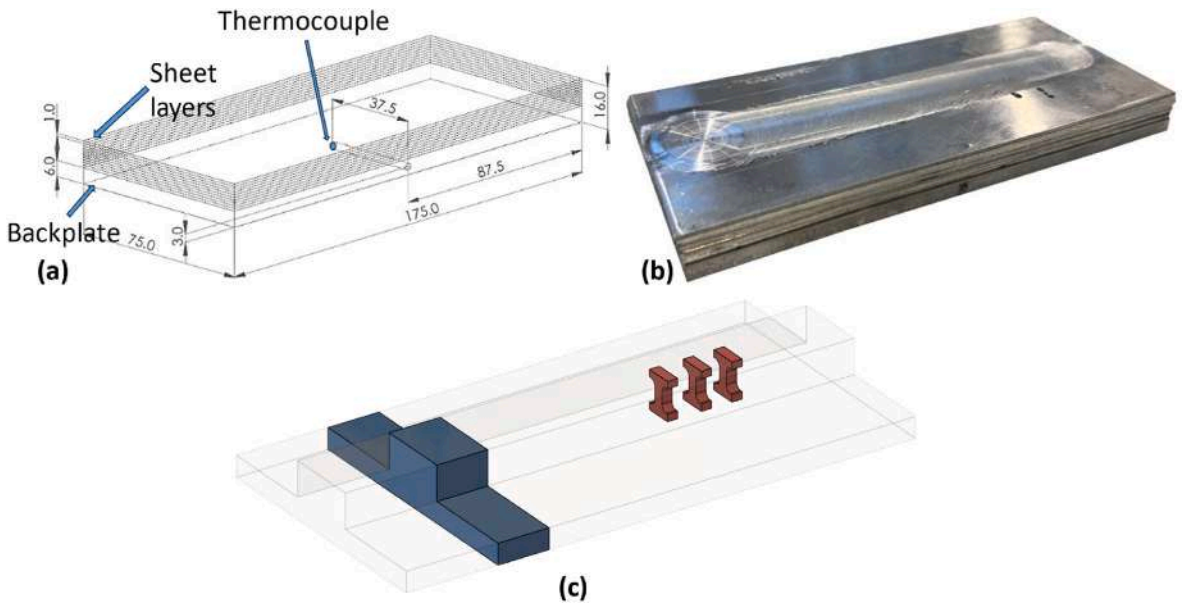

Fig. 2. (a) Sketch of the process with thermocouple position, (b) completed build – 1100 rpm, (c) and Schematic representation of the specimens prepared for mechanical characterization tests.

Table 1
Tool geometries used for the energy consumption comparison.

Sheet thickness [mm]	Shoulder diameter [mm]	Pin major diameter [mm]	Pin height [mm]
2	10	5.0	3
3	12	5.5	4
4	15	6.0	5
5	20	8.0	6

backplate, was obtained from each build according to ASTM/E8 standards. Engineering stress and engineering strain results were collected to evaluate the Ultimate Tensile Test (UTS) and the Elongation to Fracture (ETF). The tests were conducted on a Galdabini Quasar 60 machine using a loading speed of 1 mm/min quasi-static tensile. Finally, microhardness tests were carried out on the cross-section along five vertical lines, equally spaced from the specimen center of 5 mm, with a vertical pitch of 1 mm.

3. Results

3.1. Mechanical properties

First, the produced builds were analyzed by OM and SEM. Only the specimens corresponding to tool rotation of 700, 900, and 1100 rpm were considered. The specimen welded with 500 rpm failed during the saw cutting, with separation of the layers, as the "cold" welding conditions did not allow for sound solid bonding to occur. On the contrary, the high heat input of the 1300 rpm test resulted in excessive distortion and sheets burst through the bottom during welding (Fig. 3).

For each cross-section, the bonded area boundary was identified by SEM observation, in order to exclude the zones in which the initial sheet separation was still visible, i.e. proper bonding conditions were not reached (close up 2 in Fig. 3). Increasing area is found with increasing heat input, i.e. increasing tool rotation. The extension of the welded areas, highlighted with yellow dotted lines, are 173.08, 191.48, and 211.50 mm^2, for the 700, 900, and 1100 rpm case studies, respectively.

During the tests, temperatures were acquired for each layer. Fig. 4a shows the temperature histories for the 1100 rpm case study, while in Fig. 4b the average peak temperatures are reported for all case studies

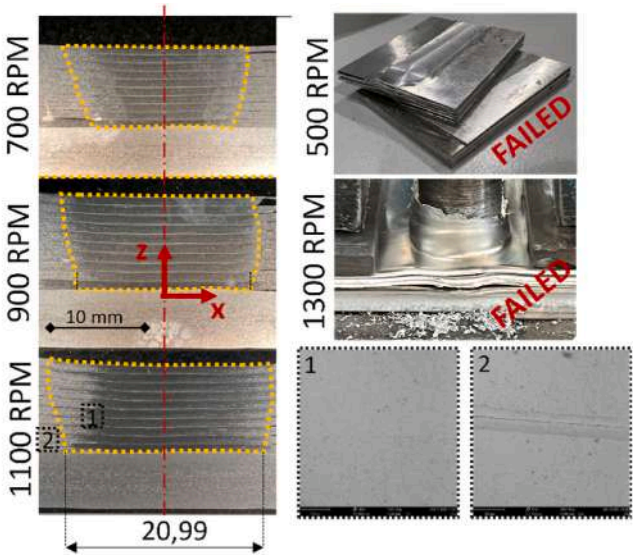

Fig. 3. An etched cross section highlighting the actual welded area for 700, 900, and 1100 rpm case studies and SEM close-up (1) inside and (2) outside the welded area. Failed 500 and 1300 rpm tests.

and layers. It is noted that the 1300 rpm build was interrupted after 6 layers for the above-mentioned reasons.

Apart from the first layer, welded with tool rotation of 2200 rpm for all case studies, as expected a decreasing temperature is measured at mid-thickness of the backplate with increasing layer number and decreasing tool rotation. Two interesting observations can be made on the temperature data: first, each sheet undergoes several thermal cycles; in particular, layer position L (including the backplate, L = 0) undergoes 10-L thermal cycles with peak temperatures not lower than about 300 °C. Then, a cut-off temperature can be identified, for each layer, based on the values measured for the 500-rpm case study, corresponding to insufficient heat conditions. Mechanical tests were carried out to assess the effectiveness of the bonding conditions reached. First, bending tests were conducted to investigate the potential occurrence of delamination between the welded layers and between the first layer and the

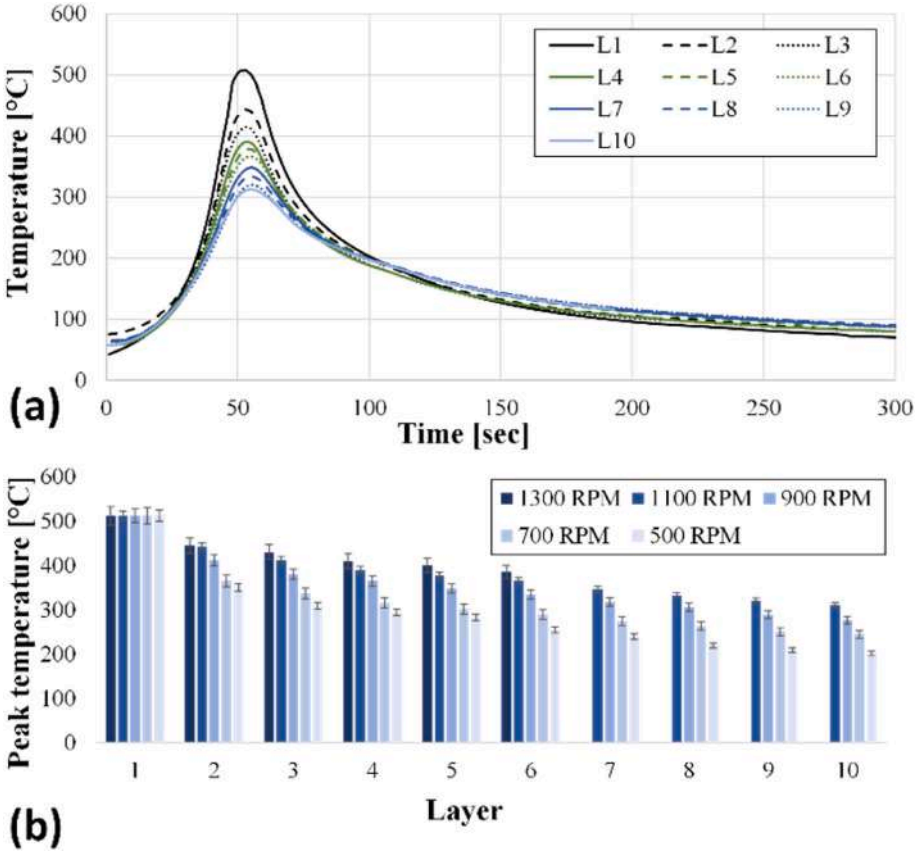

Fig. 4. (a) Temperature profiles for the ten layers – 1100 rpm and (b) effect of tool rotation on the average peak temperature for each layer.

backplate, in order to highlight inadequate bonding conditions. Fig. 5 shows the bending test results for the considered case studies as compared to the base material (BM, machined from solid bar).

It is observed that similar performances are obtained for the three considered case studies, indicating that the effectiveness of the solid bonding achieved is not heavily affected by the heat input. Looking at the base material, a larger peak load value, and lower ductility are observed. This can be explained by considering the thermal histories during the process. Both AA5754-H22 and AA5083-H111 are work-hardened alloys, and the effect of the hardening is lost, both in the backplate and the layer sheets, because of the recovery induced during the process. As shown in Fig. 5b, the failure occurs in the backplate with a nearly 45° crack. For this reason, the backplate material, i.e. AA5083-H111, was used as BM. The work hardening routine corresponding to H111 results in slightly higher yield and UTS and ETF lower than O conditions, thus explaining the different behavior observed. The micro-mechanical properties of the builds were assessed by HV measurements. Fig. 6 shows the HV measured in a cross-section along five vertical lines equally spaced with a horizontal pitch of 5 mm with respect to the center of the specimen (−10, −5, 0, +5, +10 on x-axis, Fig. 3) and with a vertical pitch of 1 mm (z-axis, Fig. 3).

It is worth noting that the point corresponding to z = 0 lies on the backplate. For this reason, values higher than the ones measured for the other points which, in turn, are taken at the mid-thickness of each layer, are found. As the HV values are regarded, they fall in the range of 65–80 HV, which is lower than the hardness of the AA5083-H111 base material, confirming the observations made for the bending tests. Additionally, looking at Fig. 6a it can be observed that most of the hardness

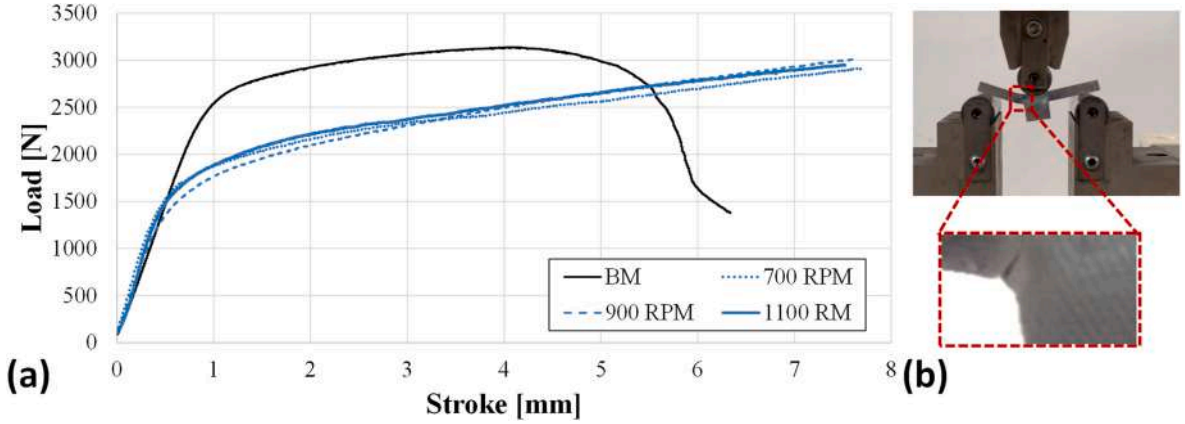

Fig. 5. (a) Bending test results and (b) failure mode for all specimens.

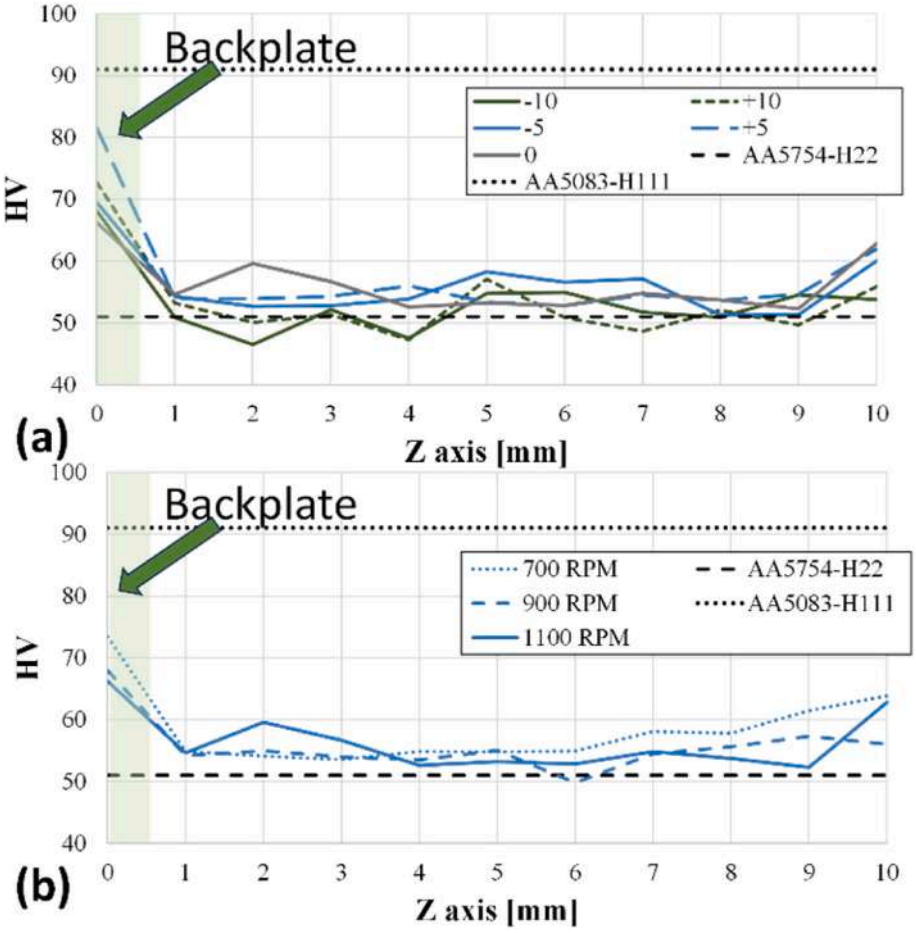

Fig. 6. (a) Microhardness along five vertical measurement lines – 1100 rpm case study, and (b) effect of tool rotation on the microhardness for each layer at the center line (x = 0).

values measured in the different layers are larger than the hardness of the base material. This is common for FSW of work-hardenable alloys, which, differently from precipitation-hardenable alloys, do not lose hardness because of precipitation dissolution during the process and experience only the beneficial effect of grain refinement due to CDRX. The lowest HV values, close to the hardness of the parent material, are found for the x-10 curve, corresponding to the retreating side of the joints. It is also noted that the values vary in a relatively small range, i.e. about 48–58 HV, indicating homogeneous conditions in the build both in the horizontal and vertical direction. Finally, it is noted that slightly larger values are found in the last layer for every x value. This is because the last layer does not undergo further thermal cycles after welding. In this way, the smallest grain size is expected as no grain growth phenomena occurred in this zone. The hardness profiles obtained with varying tool rotation at x = 0 are shown in Fig. 6b. The results confirm the observations made for the bending tests, i.e. the effect of the tool rotation on the mechanical performance of the joints is limited.

To further investigate the effectiveness of the produced builds, tensile tests were carried out (Fig. 7).

It is observed that the variations in mechanical properties with respect to the base material (dashed lines in Fig. 7) are relatively small, with UTS values of 96 %, 95 %, and 91 % and ETF values of 96.7 %, 97.3 %, and 99.3 % for 700 rpm, 900 rpm, and 1100 rpm, respectively. It is well known that in solid bonding-dominated processes the increased heat input results in enhanced grain growth with a consequent decrease in mechanical efficiency and an increase in ductility (Buffa et al., 2014).

Considering that the bending resistance is comparable between the different tool rotations, and the mechanical strength is always higher

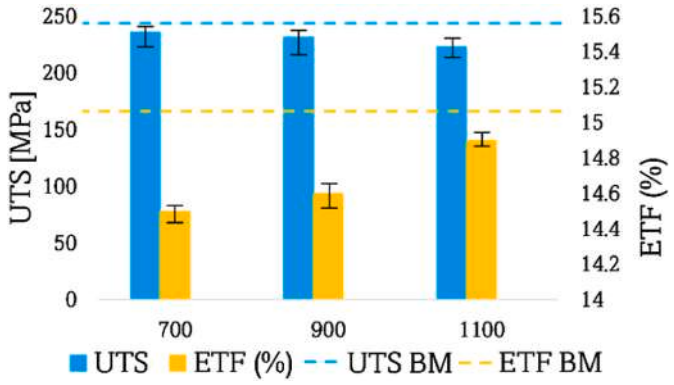

Fig. 7. Tensile test results in terms of UTS and ETF for the considered case studies and UTS and ETF of base material.

than 90 %, which can be considered a good result for solid bonding processes based on the existing literature (Mishra and Ma, 2005), the only driver for the choice of the benchmark was the extension of the welded area. The latter varies more significantly than the mechanical properties with tool rotation and can significantly affect environmental performances. Based on the above observations, the specimen obtained with tool rotation of 1100 rpm was selected for the energy comparison, being the one that allows for a larger welded area without a large loss of mechanical performance. Additionally, the minimum welded area width measured, i.e. 20.99 mm (see again Fig. 3) was used to select the width

of 20 mm as a reference for the subsequent analyses. Finally, it can be observed that the mechanical results are consistent with the ones reported by other authors for FSAM of 5 xxx series. Specifically, UTS efficiency in the range 89–99 % can be achieved by FSAM (Zhu et al., 2023).

3.2. Energy demand assessment

For each case study, the electrical energy demand was acquired. Specifically, the power-time data was collected by connecting a three-phase electrical network to the input electrical connection of the ESAB machine. The power was measured for the entire wall building. In particular, for each single sheet addition, both the FSAM as well as the milling step were monitored and included in the electrical energy demand calculation. An example of collected power vs. time curve by pinless FSAM for one sheet addition is reported in Fig. 8. In this figure, the FSAM and the milling steps are clearly visible along with non-productive production modes such as tool change and CNC program launching. In this study, only the pure productive modes have been considered for the energy demand quantification. In other words, only the areas corresponding to the FSAM step and Milling step time spans in Fig. 8 were calculated. This choice was driven by the lack of industrial practices and data concerning non-productive operations (tool change, clamping of a new sheet, etc.). Once the power trends vs. time were acquired for each added sheet layer, the energy consumption was then calculated from the power-time graph by direct numerical integration method.

The energy demand of the pinless approach was compared to that of the conventional FSAM approach. For the pinless case, only the energy performances concerning the 1100 rpm case are discussed, as previously mentioned. Four different thicknesses were considered as reported in paragraph 2. For each thickness, the number of required passes per layer has been calculated considering a tool shoulder overlap equal to 80 % (Jiang et al., 2023). For each configuration, the energy for a single pass was experimentally acquired, while the number of passes required was fixed based on the literature (Zhang et al., 2012). The energy demand results of all the different analyzed process configurations are summarized in Table 2.

In Table 2 a unit metric is also listed to define the required energy for 1 mm of built wall height (mm_h) for a given width of the wall, i.e. 20 mm. By analyzing this metric, it is possible to note that the energy efficiency of the conventional FSAM approach increases with increasing sheet thickness. The pinless approach outperforms the conventional one in the case of 2 and 3 mm, while for the case of 4 and 5 mm the conventional FSAM provided the best performance. In Fig. 9 the energy demand of the analyzed FSAM approaches is reported as a function of the height of the manufactured wall.

It is worth remarking that, for a given target wall height to be produced, only sheets of the same thickness are assumed to be used. Under this assumption, not all the wall heights are possible to be manufactured

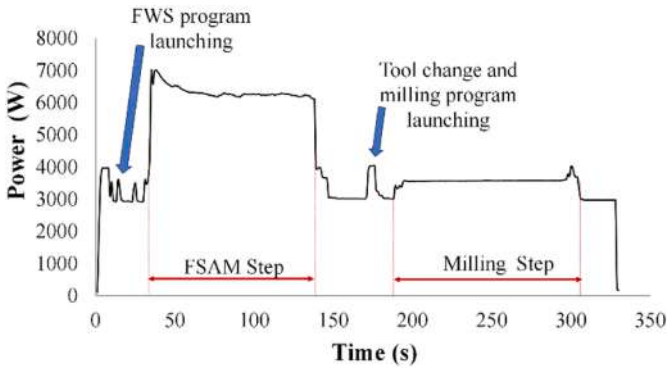

Fig. 8. Electric power trend of single sheet addition - 1100 rpm.

Table 2
Energy data for the analyzed FSAM processes.

Process	FSAM first sheet addition (kWh)	FSAM single pass Energy (kWh)	Milling step Energy (kWh)	Tool passes per layer	Specific Energy (E/mm_h)
Pinless FSAM	0.247	0.200	0.071	1	0.275
FSAM th 2 mm	N.A	0.158	0.071	8	0.667
FSAM th 3 mm	N.A	0.167	0.071	7	0.413
FSAM th 4 mm	N.A	0.175	0.071	6	0.280
FSAM th 5 mm	N.A	0.188	0.071	5	0.202

for a selected thickness. In fact, the FSAM approach can be used for reusing sheet metal scraps; as within a single company the range of the used sheet thicknesses is very narrow, it seems fair considering one single thickness for the FSAM approach implementation.

It is possible to conduct two distinct analyses that identify two different industrial scenarios. In the first case, the company focuses on producing walls using single-thickness sheets. In the second case, the company aims to produce walls using varying thicknesses, starting from the four thicknesses analyzed in the traditional FSAM approach (2, 3, 4, and 5 mm). These two industrial strategies will be compared with the pinless FSAM approach carried out with 1 mm thick sheets. For both industrial scenarios, the goal is to achieve different wall heights with incremental steps equal to 1 mm.

3.2.1. Single-thickness approach

Following this approach, constructing x mm of height can be achieved using n sheets x/n mm thick. This method requires the milling phase to eliminate any intralayer imperfections without the need to remove the remaining excess material. As an example, using 3 mm thick sheets to build an 8 mm wall, three elements would be necessary, involving intermediate milling to reduce any surface irregularities, and finally, the removal of the 1 mm of remaining excess material. A dry machining condition with 400 mm/min of Feed Rate is considered, resulting in a processing time of 26.25 s. It is assumed that 1 mm of material is removed in each condition of excessive material. Hence, the Material Removal Rate (MRR) results equal 0.5 cm^3/s. The results presented in (Kara and Li, 2011) and (Priarone et al., 2020) were used to estimate the electrical energy consumption for the machining steps. These studies provide Specific Energy Consumption (SEC) curves as a function of MRR for three different machines (Fadal, Mori, and Dura). Considering the aforementioned MRR, the three SEC values were calculated and the average value, equal to 0.03057 kWh, was used for the following analyses. Fig. 10 shows the Electrical Energy required for the production of different wall heights.

It is possible to observe a “sawtooth” pattern for traditional FSAM. For instance, when analyzing the case of 2 mm sheets, starting from an even number as wall height, a significant amount of energy must be provided, due to the necessity of using a new sheet, increasing the total thickness of 2 mm, and a machining step for 1 mm removal. In turn, starting from an odd number as wall height, a slight decrease is observed since the target height is reached using only the FSAM phases. The sawtooth pattern becomes more pronounced with increasing sheet thickness. For example, considering a thickness of 5 mm, to reach a target height of 11 mm, three sheets must be used, but it will be necessary to remove 4 mm of material. This results in higher energy consumption compared to the case where the target height is 14 mm.

It can be observed that for heights of 4, 8, and 11 mm, considering FSAM 4 mm, FSAM 5 mm, and pinless FSAM, a few break-even points are obtained. The pinless FSAM approach suggested in this work is always advantageous in terms of energy consumption when compared to

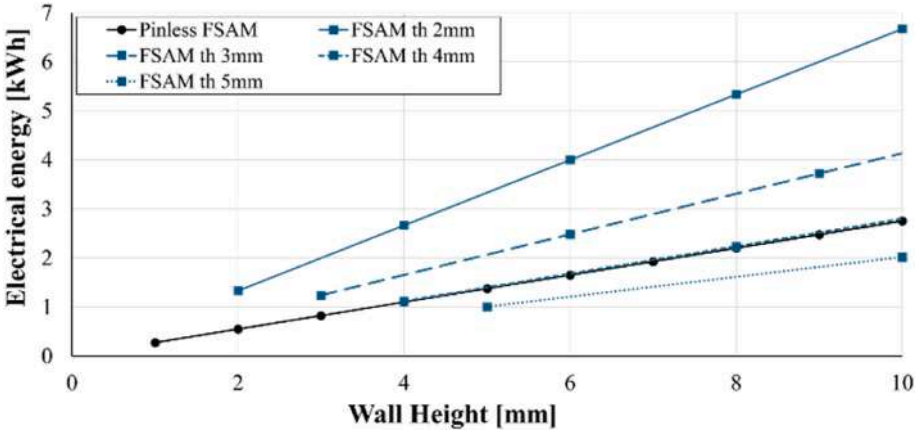

Fig. 9. Electrical Energy demand of the analyzed FSAM process as a function of the manufactured wall height.

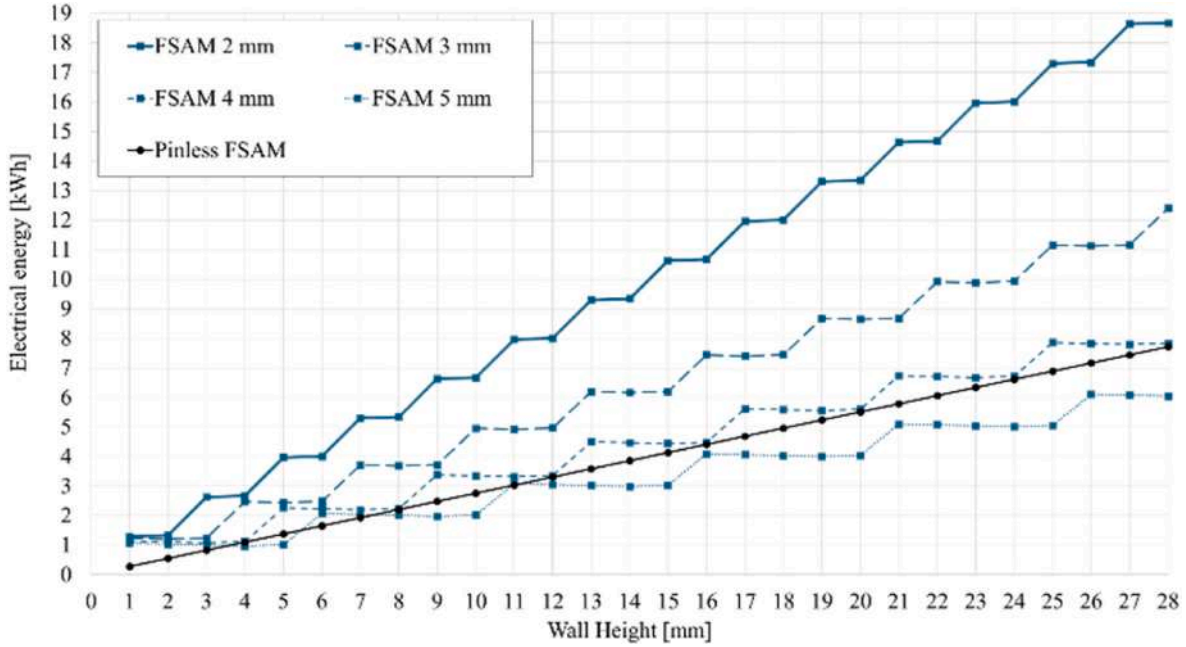

Fig. 10. Electrical Energy demand of the analyzed FSAM processes as a function of the manufactured wall height (ΔH = 1 mm).

FSAM 2 mm, FSAM 3 mm, and FSAM 4 mm, except for the previously indicated break-even points. When compared to the FSAM 5 mm approach, it is advantageous below the height of 11 mm, except for heights of 4, 5, 8, 9, and 10 mm. Beyond the height of 11 mm, the FSAM 5 mm approach is always preferable.

3.2.2. *Multi-thicknesses approach*

In the multi-thickness approach, the target height H can be achieved without the need for material removal operations. Therefore, it was necessary to find, among all possible combinations that allow reaching the target height, the one that requires the least amount of electrical energy for its realization. The problem of identifying all possible combinations that allow reaching the target height is known as a variant of the Subset Sum Problem. Given a set of available sheet thicknesses $S = \{s_1, \ldots, s_n\}$ and a target height H, all possible combinations of elements C can be identified using Eq. (1).

$$\sum_{s \in C} s = H \qquad \text{Eq. 1}$$

This problem was implemented in MATLAB (version R2022a) using an iterative backtracking algorithm. The script outputs a matrix where each row contains the number of sheets of thicknesses 2, 3, 4, and 5 mm to be used to achieve the height H_i. By associating an energy value with each sheet thickness, representing the energy required to process it using the traditional FSAM technique, all electrical energy values for all combinations are calculated. A command line was added to this script to identify the combination with the lowest energy value among all the rows. Fig. 11 shows the comparison between the electrical energy required for different wall heights, for the pinless approach and best the multi-thickness approach.

A "sawtooth" pattern can also be observed in this case. However, the advantage of using the pinless FSAM process increases for heights below 16 mm. Fig. 12 shows the number of elements used for each type of sheet to achieve various heights up to 28 mm.

As can be observed, heights above 6 mm can all be achieved, following the presented logic, by combining sheets with thicknesses of 2, 4, and 5 mm. Additionally, as the target height increases, there is an increasing use of 5 mm thick sheets. Being the break-even for this approach a value larger than the one found for the single sheet approach with 5 mm sheets, it can be stated that, due to the negligible energy consumption of the milling phase with respect to the welding phase, the single-thickness approach with large thickness sheets is the most

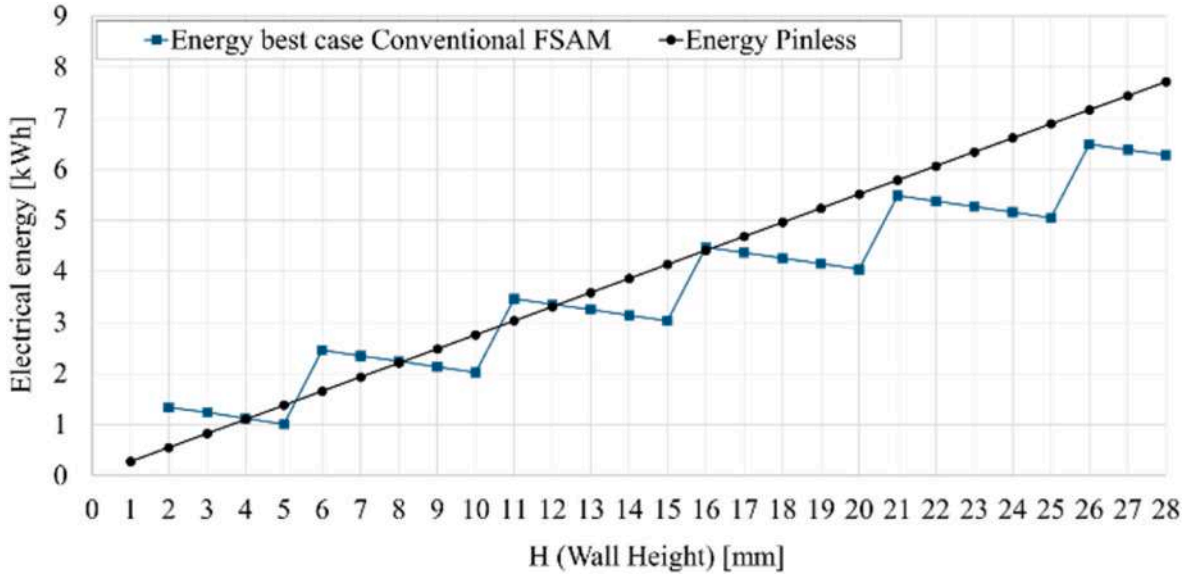

Fig. 11. Comparison of Electrical Energy Required Between pinless FSAM and Traditional FSAM Considering the Best Possible Combination Based on Different Heights Achievable (ΔH = 1 mm).

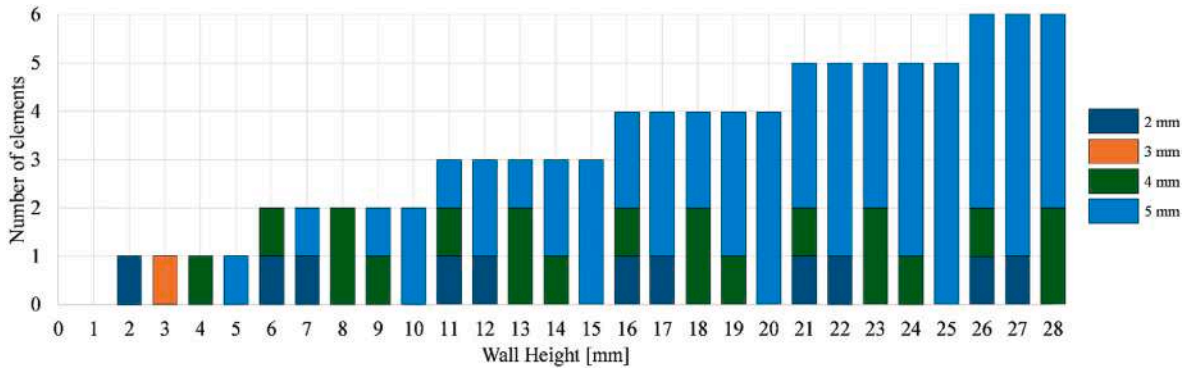

Fig. 12. Number of elements and types of sheets used to achieve different target heights.

favorable under the energy consumption point of view.

4. Life Cycle Assessment comparative analysis

This section describes the developed LCA analysis, including the goal and scope, functional unit, systems boundaries, and the life cycle inventory analysis as suggested by the ISO (14040). The LCA analysis aims to account for the difference in terms of energy and used material of two different solid-state additive manufacturing approaches: single-thickness traditional FSAM and pinless FSAM.

It is worth noting that for the traditional single-thickness FSAM approach, only the 4 mm and 5 mm cases will be thoroughly discussed; in fact, smaller thickness options provide worse environmental performance even considering only electrical energy as a metric. Including the environmental impact reduction due to a lower material consumption characterizing the pinless approach, would just confirm what is already shown in Fig. 10. Following the same reasoning, also the multi-thickness approach is left out of the analysis; actually, this approach and the pinless option differ only for the processing electrical energy consumption while demanding the same amount of material.

4.1. Goal and scope

LCA analysis conducted in this study aims to investigate and compare the environmental impact of the traditional single-thickness FSAM and pinless FSAM processes. This analysis would allow the more environmentally friendly process to be identified by varying the height of the wall to be manufactured.

Moreover, the LCA analysis allows the contribution of the factors affecting the environmental impact of these processes to be identified. To be more specific, the share of each factor (deposition electricity, machining electricity, material-related impacts) towards the total impact can be identified.

4.2. Functional unit

The functional unit chosen for the analysis is the mass of the AA5754 aluminum sheet used to manufacture a given target height. The height varied from 10 mm to 28 mm with a 1 mm increment step, therefore 19 LCA analyses were launched. This range was selected as directed.

4.3. System boundary and Life Cycle Inventory (LCI)

The objective of the LCA study is to assess the environmental performance of the traditional FSAM single-thickness approach and pinless FSAM, leading to a comparative analysis of the two methods. For each approach, the impact of the involved material and the processing of electrical energy is considered.

All the steps reported in Fig. 13 a, b, and c have been included in the analysis. Specifically, part of the modeling effort was addressed to the sheet production manufacturing step. According to the Recycled Content approach (Hammond et al., 2011) it was assumed that a fraction (R = 45 %) (Granta Design Limited, 2023) of the input aluminum comes from secondary production. Therefore, the system boundaries include an initial ingot consisting of 55 % material from primary production and 45 % from secondary production. The secondary production, based on scrap remelting, was modeled using EEA data European Aluminium Environmental Profile Report (European Aluminum, 2018). Moreover, the permanent losses due to oxidation characterizing scraps remelting were accounted for by adding 16 % of primary aluminum as suggested by (Duflou et al., 2015). After the remelting step, the sheet production step takes place. In this step, the ingot undergoes homogenization and pre-heating at a temperature of 500 °C before being processed by hot and cold rolling. Also, for the sheet production step, the inventory is based on the data available from the European Aluminum Association (EAA) (European Aluminum, 2018). The modeled flows, including the material scraps to produce 1 kg of aluminum alloy sheet, are reported in Fig. 13a. The rolled sheet was used as input for modeling the actual wall production by the two considered approaches. An example of the considered energies and material flows included in the models are reported in Fig. 13b and c. It is worth noticing that the common impacts (factors affecting both processes equally) have not been included in the analyses: the sheet needed for the clamping that results in process scraps after the "clamping sheet removal step" and the related processing energy (electrical energy for performing the cutting operations).

The pinless and traditional FSAM processing, as well as the machining energy, were quantified as described in section 3.2.

4.4. Interpretation of the results

The LCA models were implemented in SimaPro, and both Single scores (CED and GWP100) and Endpoint ReCiPe 2016 (H) analyses were developed. The developed models, for the case of a 12 mm height wall, result in the CED networks shown in Fig. 14. It can be noted that the impact of the material is higher than that concerning electrical energy use. Also, such an effect is higher for the traditional FSAM causing a worse environmental performance. The higher impact is due to the extra material (from 15 mm to 12 mm height) to be removed to reach the target height.

As an example of the output analyses, the results for the 12 mm case when compared to 1–5 mm Traditional FSAM are reported in Figs. 15–17. It can be observed that the considered trend of output metrics is proportional and that pinless FSAM and 4 mm Traditional FSAM provide the best performances. For the sake of clarity from now on only the results concerning the CED will be discussed.

IPCC Global Warming Potential (GWP) 100a, reported in Fig. 17, and the ReCiPe Endpoint (H) method in Fig. 18, show the same trends.

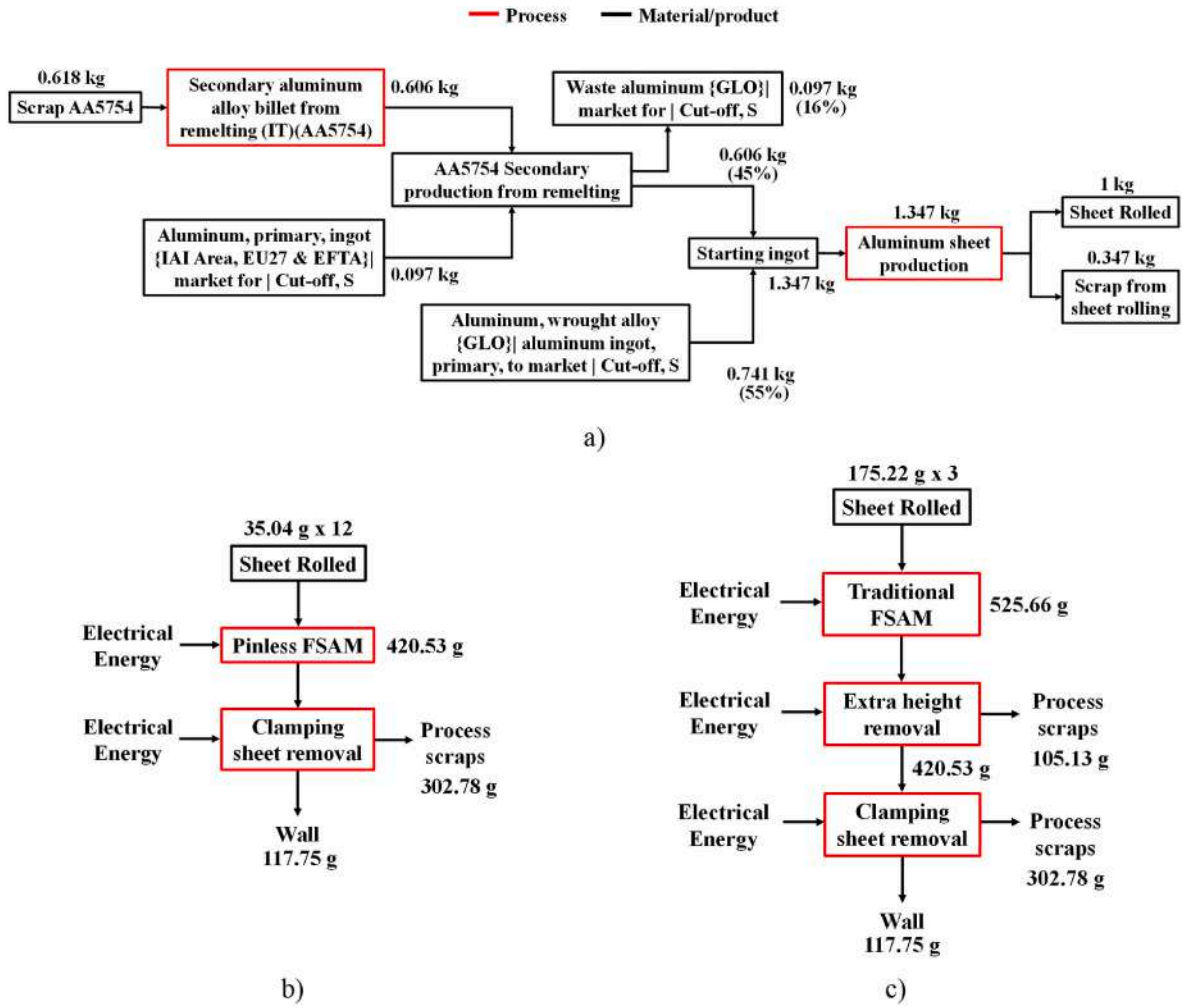

Fig. 13. Steps and processes for the production of 1 kg of sheet (a) and example of Energy and materials flows for the pinless FSAM (b) and traditional FSAM (c) for the production of a 12 mm height wall.

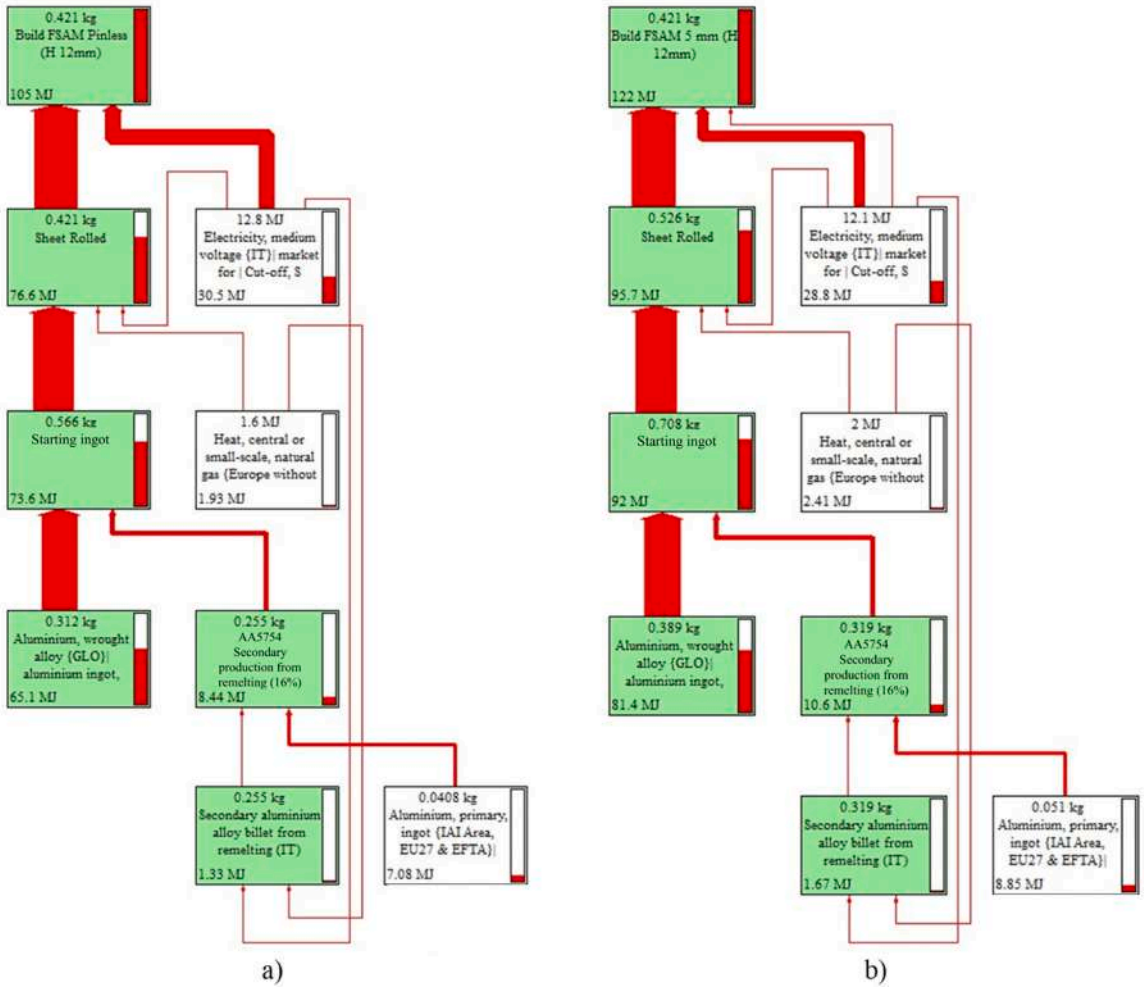

Fig. 14. Network diagrams for pinless FSAM (a) and Traditional FSAM (b) 12 mm wall case study.

4.5. The impacts of pinless FSAM and traditional FSAM

To show the environmental impact improvement of the pinless FSAM when a full LCA approach is used, the comparative CED results are reported in Fig. 18. It is possible to note that when also the impact related to the material usage is considered, the performance of the pinless FSAM improves significantly. Actually, comparing Figs. 18 and 10 it is possible to note that the 5 mm FSAM curve moves upwards and pinless FSAM outperforms the traditional approach for a larger number of possible target wall heights. For the selected heights (10–28) shown in Fig. 18, the 5 mm FSAM is the most environmentally friendly option only for 6 out of 19 cases.

5. Summary and conclusions

In the paper, an experimental approach aimed at enhancing the energy efficiency in FSAM of aluminum alloys is proposed. 1 mm thin AA5754-H22 sheets were welded on a 6 mm thick AA5083-H111 backplate with a pinless tool thus reaching large welded area widths and avoiding multiple passes per layer, which is a common routine for conventional FSAM. The mechanical properties of the builds were evaluated with varying tool rotation. Along with the technical feasibility of the new pinless approach, a comparative environmental impact analysis is developed to characterize the performance of different FSAM approaches in terms of energy and resource efficiency. This study demonstrated that mechanical performances comparable with the ones conventionally used in FSAM can be obtained with less energy and time, for most case studies. However, it is worth noting that this study focuses on a limited range of wall heights, and the results may not be directly generalized to configurations outside this range. Furthermore, although the same approach can be used for every material, if a different material is to be considered, a new comprehensive engineering assessment, similar to the approach here proposed, would be required to ensure optimal process parameters and structural performance before industrial application. Finally, similarly to FSW, this process offers a high level of safety due to its inherent characteristics, including full automation and the absence of sparks, fumes, or harmful emissions. These features not only enhance workplace safety, but also make the process more environmentally friendly and suitable for implementation in controlled industrial environments (Mori et al., 2013).

Based on the achieved results, the following conclusion can be drawn:

- ✔ The tool rotation does not heavily affect the joints' micro and macro mechanical properties, while larger tool rotation values result in larger welded area width. The 500 rpm and 1300 rpm case studies identified limiting conditions in terms of heat input;
- ✔ The best-performing configuration was selected for energy consumption comparison to conventional FSAM based on thicker sheets and multiple passes per deposited layer; in particular, the proposed pinless approach should be preferred to the conventional FSAM process carried out with sheets of thicknesses lower than 4 mm. Similar energy efficiency is found when sheet thickness is equal to 4 mm. Finally, conventional FSAM should be preferred if plates with a

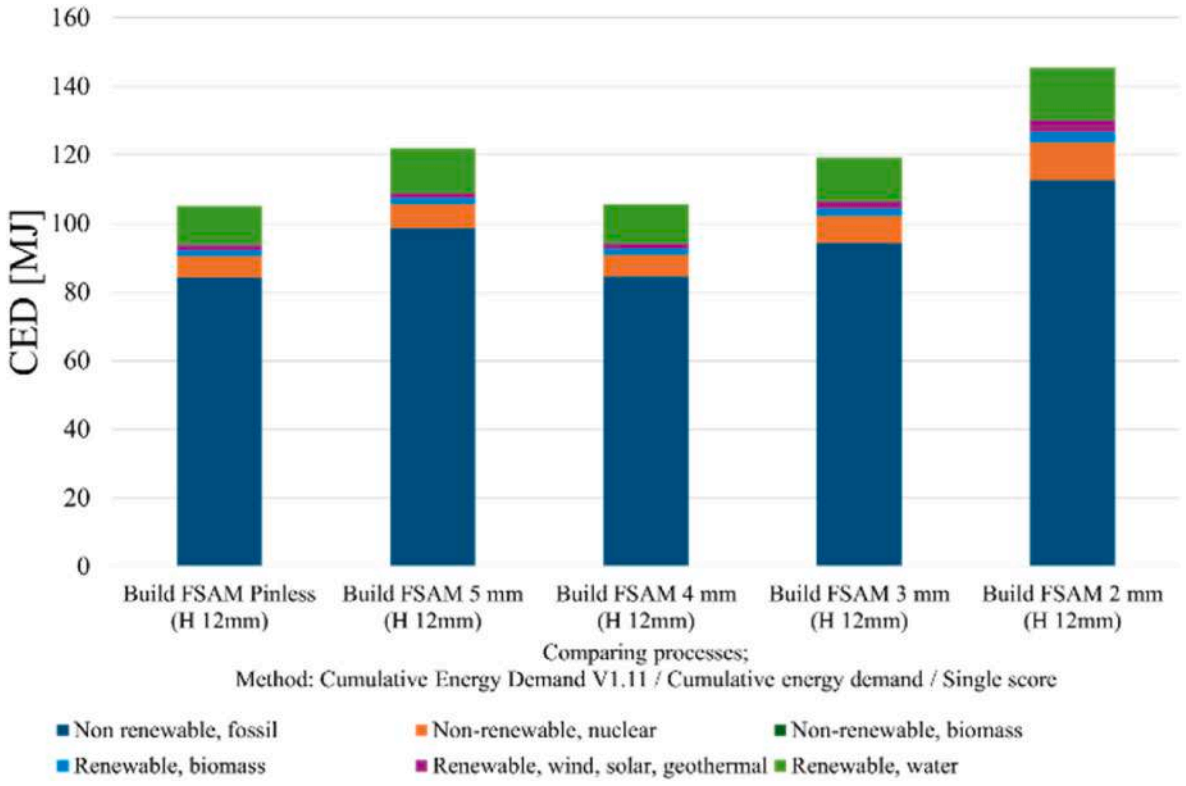

Fig. 15. CED method Single Score results (MJ) for 12 mm wall.

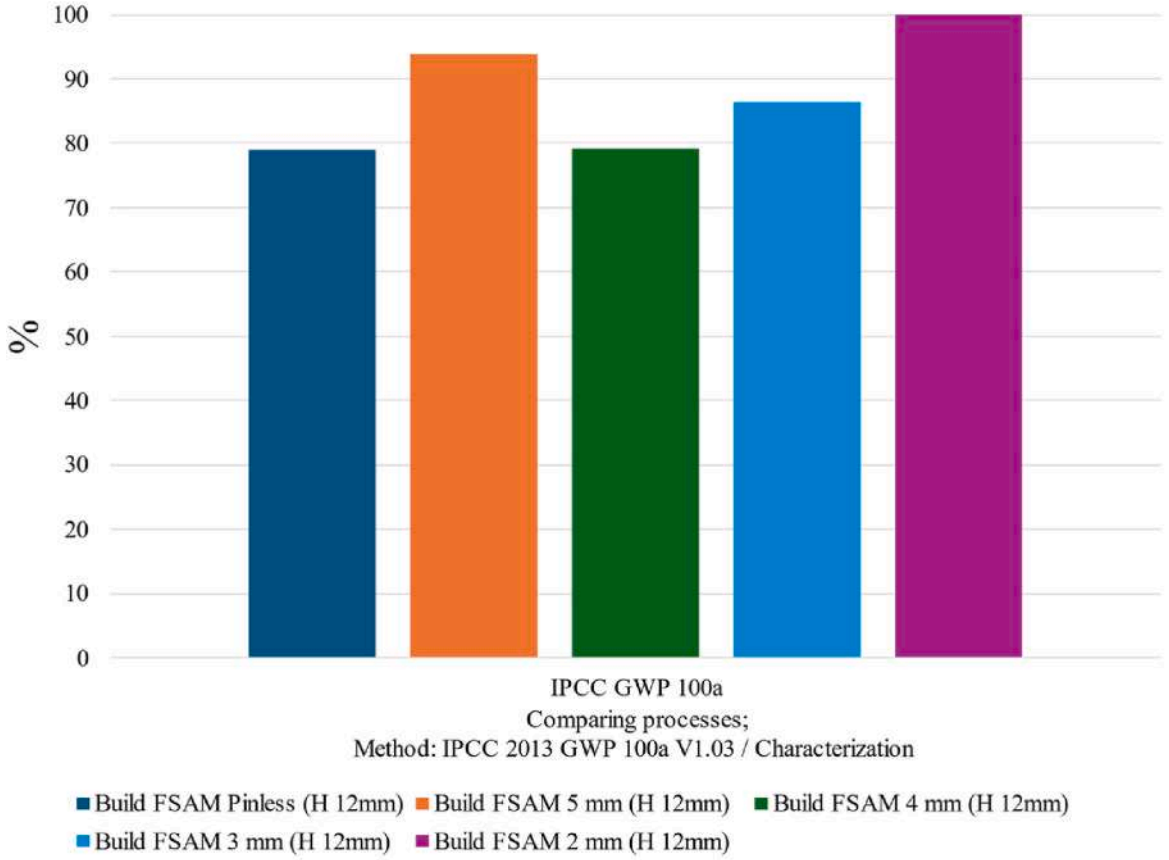

Fig. 16. GWP 100a method Characterization results (%) for 12 mm wall.

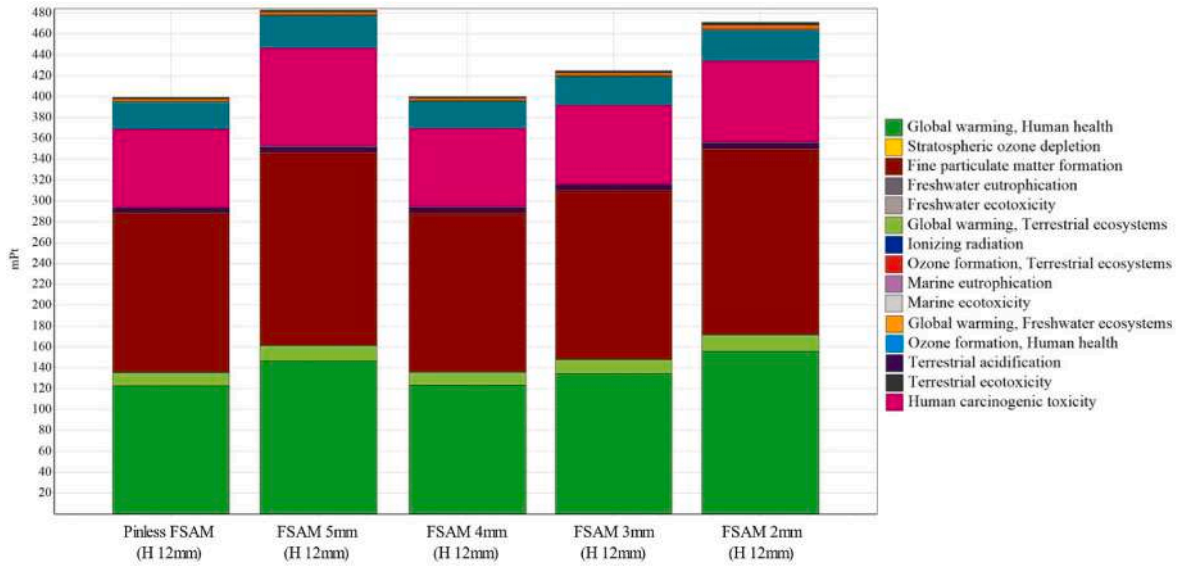

Fig. 17. LCA results (Endpoint) for 12 mm wall per impact category.

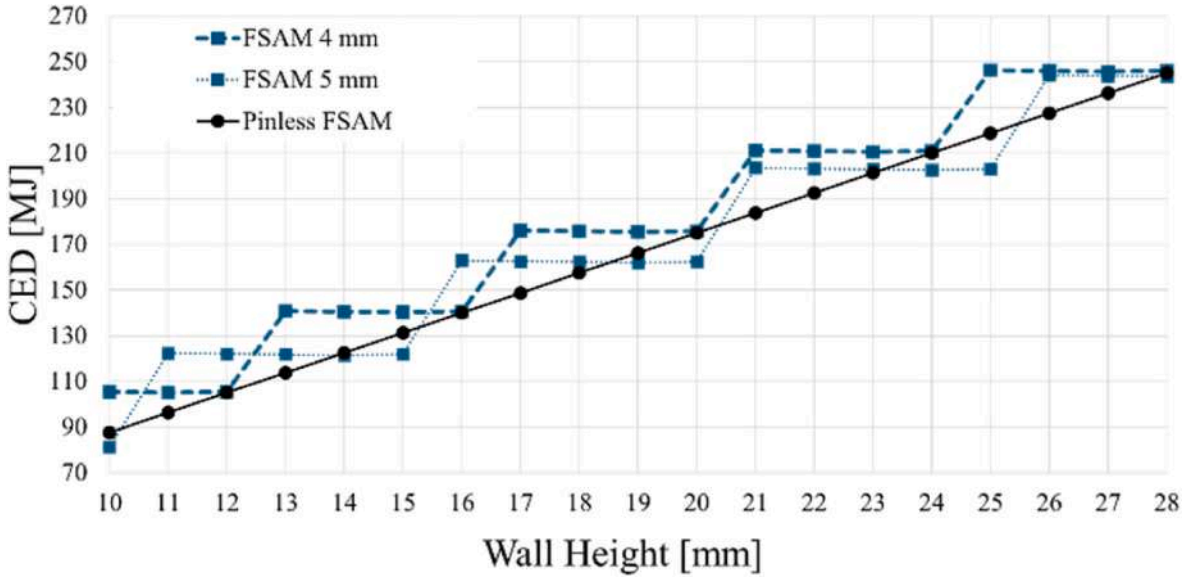

Fig. 18. Comparison of CED method Single Score results (MJ) for different wall heights using pinless FSAM and FSAM 4 and 5 mm.

thickness of 5 mm (or more) are used, taking into account only the required electrical energy;

- ✔ Following the single-thickness approach, considering the milling phase to remove the excess material, pinless FSAM is energetically disadvantageous beyond the height of 11 mm, compared to traditional FSAM of 5 mm;
- ✔ Following the multi-thickness approach, where the target height is achieved considering the milling phase only to eliminate any intra-layer imperfections, the energy consumption advantage in using the pinless FSAM process holds till heights of 16 mm;
- ✔ Comparing the results of single- and multi-thickness approaches it can be concluded that the single-thickness approach always outperforms the multi-thickness approach;
- ✔ As pinless and traditional FSAM is characterized by different amounts of involved material, a full LCA analysis was developed to take into account such factors of influence properly. The analysis reveals that the performance of the pinless FSAM improves significantly as it becomes the most environmentally friendly option for the majority of the analyzed wall heights.

Future work will be focused on the analysis of the static and dynamic mechanical properties, the energy demand, and the process cost effectiveness as a function of additional process parameters, such as feed rate and vertical load, and different aluminum alloys.

CRediT authorship contribution statement

Gianluca Buffa: Writing – review & editing, Methodology, Conceptualization. **Simone Amantia:** Writing – original draft, Software, Investigation. **Davide Campanella:** Visualization, Investigation, Formal analysis. **Giuseppe Ingarao:** Writing – review & editing, Methodology, Conceptualization. **Livan Fratini:** Supervision, Funding acquisition, Conceptualization.

Funding

This study was carried out within the MICS (Made in Italy – Circular and Sustainable) Extended Partnership and received funding from the European Union Next-Generation EU (PIANO NAZIONALE DI RIPRESA E RESILIENZA (PNRR) – MISSIONE 4 COMPONENTE 2, INVESTIMENTO 1.3 – D.D. 1551.11–10-2022, PE00000004). This manuscript reflects only the authors' views and opinions, neither the European Union nor the European Commission can be considered responsible for them.

Declaration of competing interest

The authors declare that they have no known competing financial interests or personal relationships that could have appeared to influence the work reported in this paper.

Data availability

Data will be made available on request.

References

Buffa, G., Pellegrino, S., Fratini, L., 2014. Analytical bonding criteria for joint integrity prediction in friction stir welding of aluminum alloys. J. Mater. Process. Technol. 214, 2102–2111. https://doi.org/10.1016/j.jmatprotec.2014.02.014.

Duflou, J.R., Tekkaya, A.E., Haase, M., Welo, T., Vanmeensel, K., Kellens, K., Dewulf, W., Paraskevas, D., 2015. Environmental assessment of solid state recycling routes for aluminium alloys: can solid state processes significantly reduce the environmental impact of aluminium recycling? CIRP Annals 64, 37–40. https://doi.org/10.1016/J.CIRP.2015.04.051.

European Aluminum, 2018. Environmental profile report. https://www.european-aluminium.eu/resource-hub/environmental-profile-report-2018/, 7.17.24.

Gotawala, N., Yu, H.Z., 2023. Material flow path and extreme thermomechanical processing history during additive friction stir deposition. J. Manuf. Process. 101, 114–127. https://doi.org/10.1016/J.JMAPRO.2023.05.095.

Granta Design Limited, 2023. https://www.ansys.com/it-it/products/materials/granta-edupack, 7.26.24.

Hammond, G., Jones, C., Lowrie, F., Tse, P., Building Services Research and Information Association., University of Bath, 2011. Embodied Carbon : the Inventory of Carbon and Energy (ICE). BSRIA.

Hu, F., Chen, G., Lin, Y., Wang, H., Zhu, Z., 2024. Numerical and experimental study on the thermal process during additive friction stir deposition. CIRP J. Manuf. Sci. Technol. 48, 55–66. https://doi.org/10.1016/j.cirpj.2023.12.002.

Jiang, T., Jiao, T., Dai, G., Shen, Z., Guo, Y., Sun, Z., Li, W., 2023. Microstructure evolution and mechanical properties of 2060 Al-Li alloy via friction stir additive manufacturing. J. Alloys Compd. 935, 168019. https://doi.org/10.1016/J.JALLCOM.2022.168019.

Jones, A., Leary, M., Bateman, S., Easton, M., 2021. Effect of surface geometry on laser powder bed fusion defects. J. Mater. Process. Technol. 296, 117179. https://doi.org/10.1016/J.JMATPROTEC.2021.117179.

Kara, S., Li, W., 2011. Unit process energy consumption models for material removal processes. CIRP Annals 60, 37–40. https://doi.org/10.1016/J.CIRP.2011.03.018.

Kruth, J.P., Leu, M.C., Nakagawa, T., 1998. Progress in additive manufacturing and rapid prototyping. CIRP Ann. - Manuf. Technol. 47, 525–540. https://doi.org/10.1016/S0007-8506(07)63240-5.

Labus Zlatanovic, D., Balos, S., Bergmann, J.P., Köhler, T., Grätzel, M., Sidjanin, L., Goel, S., 2020. An experimental study on lap joining of multiple sheets of aluminium alloy (AA 5754) using friction stir spot welding. Int. J. Adv. Manuf. Technol. 107, 3093–3107. https://doi.org/10.1007/S00170-020-05214-Z/FIGURES/17.

Le, V.T., Paris, H., Mandil, G., 2017. Environmental impact assessment of an innovative strategy based on an additive and subtractive manufacturing combination. J. Clean. Prod. 164, 508–523. https://doi.org/10.1016/J.JCLEPRO.2017.06.204.

Levy, G.N., Schindel, R., Kruth, J.P., 2003. Rapid manufacturing and rapid tooling with layer manufacturing (LM) technologies, state of the art and future perspectives. CIRP Ann. - Manuf. Technol. 52, 589–609. https://doi.org/10.1016/S0007-8506(07)60206-6.

Liu, M., An, X.H., Wang, B.B., Wu, L.H., Xue, P., Liu, F.C., Ni, D.R., Xiao, B.L., Ma, Z.Y., 2024. Enhanced fatigue properties of large-scale ultrafine-grained copper fabricated by friction stir additive manufacturing and subsequent cold rolling. Int. J. Fatig. 183, 108253. https://doi.org/10.1016/J.IJFATIGUE.2024.108253.

Liu, S., Bor, T.C., Van Der Stelt, A.A., Geijselaers, H.J.M., Kwakernaak, C., Kooijman, A. M., Mol, J.M.C., Akkerman, R., Van Den Boogaard, A.H., 2016. Friction surface cladding: an exploratory study of a new solid state cladding process. J. Mater. Process. Technol. 229, 769–784. https://doi.org/10.1016/J.JMATPROTEC.2015.10.029.

Lu, I.K., Reynolds, A.P., 2021. Innovative friction stir additive manufacturing of cast 2050 Al–Cu–Li aluminum alloy. Progr. Addit. Manuf. 6, 471–477. https://doi.org/10.1007/S40964-021-00175-5/FIGURES/14.

Mishra, R.S., Ma, Z.Y., 2005. Friction stir welding and processing. Mater. Sci. Eng. R Rep. 50, 1–78. https://doi.org/10.1016/J.MSER.2005.07.001.

Mori, K.I., Bay, N., Fratini, L., Micari, F., Tekkaya, A.E., 2013. Joining by plastic deformation. CIRP Annals 62, 673–694. https://doi.org/10.1016/J.CIRP.2013.05.004.

Priarone, P.C., Pagone, E., Martina, F., Catalano, A.R., Settineri, L., 2020. Multi-criteria environmental and economic impact assessment of wire arc additive manufacturing. CIRP Annals 69, 37–40. https://doi.org/10.1016/J.CIRP.2020.04.010.

Rathee, S., Srivastava, M., Pandey, P.M., Mahawar, A., Shukla, S., 2021. Metal additive manufacturing using friction stir engineering: a review on microstructural evolution, tooling and design strategies. CIRP J. Manuf. Sci. Technol. 35, 560–588. https://doi.org/10.1016/J.CIRPJ.2021.08.003.

Rivera, O.G., Allison, P.G., Brewer, L.N., Rodriguez, O.L., Jordon, J.B., Liu, T., Whittington, W.R., Martens, R.L., McClelland, Z., Mason, C.J.T., Garcia, L., Su, J.Q., Hardwick, N., 2018. Influence of texture and grain refinement on the mechanical behavior of AA2219 fabricated by high shear solid state material deposition. Mater. Sci. Eng., A 724, 547–558. https://doi.org/10.1016/J.MSEA.2018.03.088.

Schmidt, M., Merklein, M., Bourell, D., Dimitrov, D., Hausotte, T., Wegener, K., Overmeyer, L., Vollertsen, F., Levy, G.N., 2017. Laser based additive manufacturing in industry and academia. CIRP Annals 66, 561–583. https://doi.org/10.1016/J.CIRP.2017.05.011.

Shao, J., Samaei, A., Xue, T., Xie, X., Guo, S., Cao, J., MacDonald, E., Gan, Z., 2023. Additive friction stir deposition of metallic materials: process, structure and properties. Mater. Des. 234, 112356. https://doi.org/10.1016/J.MATDES.2023.112356.

Srivastava, M., Rathee, S., 2021. Microstructural and microhardness study on fabrication of Al 5059/SiC composite component via a novel route of friction stir additive manufacturing. Mater. Today Proc. 39, 1775–1780. https://doi.org/10.1016/J.MATPR.2020.07.137.

Stubblefield, G.G., Fraser, K.A., Van Iderstine, D., Mujahid, S., Rhee, H., Jordon, J.B., Allison, P.G., 2022. Elucidating the influence of temperature and strain rate on the mechanics of AFS-D through a combined experimental and computational approach. J. Mater. Process. Technol. 305, 117593. https://doi.org/10.1016/j.jmatprotec.2022.117593.

Wang, X., Zhou, C., Luo, M., Liu, L., Liu, F., 2022. Fused plus wire arc additive manufacturing materials and energy saving in variable-width thin-walled. J. Clean. Prod. 373, 133765. https://doi.org/10.1016/j.jclepro.2022.133765.

Wits, W.W., Amsterdam, E., 2023. Fatigue prediction and life assessment method for metal laser powder bed fusion parts. CIRP Annals 72, 129–132. https://doi.org/10.1016/J.CIRP.2023.03.011.

Yi, L., Glatt, M., Thomas Kuo, T.Y., Ji, A., Ravani, B., Aurich, J.C., 2020. A method for energy modeling and simulation implementation of machine tools of selective laser melting. J. Clean. Prod. 263, 121282. https://doi.org/10.1016/J.JCLEPRO.2020.121282.

Zhang, Y.N., Cao, X., Larose, S., Wanjara, P., 2012. Review of tools for friction stir welding and processing. Can. Metall. Q. 51, 250–261. https://doi.org/10.1179/1879139512Y.0000000015.

Zhao, Z., Yang, X., Li, S., Li, D., 2019. Interfacial bonding features of friction stir additive manufactured build for 2195-T8 aluminum-lithium alloy. https://doi.org/10.1016/j.jmapro.2019.01.042.

Zhu, Z., Hu, Z., Seet, H.L., Liu, T., Liao, W., Ramamurty, U., Ling Nai, S.M., 2023. Recent progress on the additive manufacturing of aluminum alloys and aluminum matrix composites: microstructure, properties, and applications. Int. J. Mach. Tool Manufact. 190, 104047. https://doi.org/10.1016/J.IJMACHTOOLS.2023.104047.